Monthly Notices of the ROYAL ASTRONOMICAL SOCIETY

MNRAS **498,** L35–L39 (2020) doi:10.1093/mnrasl/slaa125

The 2020 April–June super-outburst of OJ 287 and its long-term multiwavelength light curve with *Swift*: binary supermassive black hole and jet activity

S. Komossa,[1★] D. Grupe,[2] M. L. Parker,[3] M. J. Valtonen,[4,5] J. L. Gómez,[6] A. Gopakumar[7] and L. Dey[7]

[1]*Max-Planck-Institut für Radioastronomie, Auf dem Hügel 69, D-53121 Bonn, Germany*
[2]*Department of Physics, Earth Science, and Space System Engineering, Morehead State University, 235 Martindale Dr, Morehead, KY 40351, USA*
[3]*European Space Agency (ESA), European Space Astronomy Centre (ESAC), E-28691 Villanueva de la Canada, Madrid, Spain*
[4]*Finnish Centre for Astronomy with ESO, University of Turku, FI-20014 Turku, Finland*
[5]*Department of Physics and Astronomy, University of Turku, FI-20014 Turku, Finland*
[6]*Instituto de Astrofísica de Andalucía-CSIC, Glorieta de la Astronomía s/n, E-18008 Granada, Spain*
[7]*Department of Astronomy and Astrophysics, Tata Institute of Fundamental Research, Mumbai 400005, India*

Accepted 2020 July 6. Received 2020 July 3; in original form 2020 May 30

ABSTRACT

We report detection of a very bright X-ray–UV–optical outburst of OJ 287 in 2020 April–June, the second brightest since the beginning of our *Swift* multiyear monitoring in late 2015. It is shown that the outburst is predominantly powered by jet emission. Optical–UV–X-rays are closely correlated, and the low-energy part of the *XMM–Newton* spectrum displays an exceptionally soft emission component consistent with a synchrotron origin. A much harder X-ray power-law component ($\Gamma_x = 2.4$, still relatively steep when compared to expectations from inverse Compton models) is detected out to 70 keV by *NuSTAR*. We find evidence for reprocessing around the Fe region, consistent with an absorption line. If confirmed, it implies matter in outflow at ∼0.1c. The multiyear *Swift* light curve shows multiple episodes of flaring or dipping with a total amplitude of variability of a factor of 10 in X-rays, and 15 in the optical–UV. The 2020 outburst observations are consistent with an after-flare predicted by the binary black hole model of OJ 287, where the disc impact of the secondary black hole triggers time-delayed accretion and jet activity of the primary black hole.

Key words: galaxies: active – galaxies: jets – galaxies: nuclei – quasars: individual: (OJ 287) – X-rays: galaxies.

1 INTRODUCTION

The last few years have seen the first direct detection of high-frequency gravitational waves (GWs) from merging stellar-mass black holes (BHs; e.g. Abbott et al. 2016, 2019). Coalescing supermassive binary black holes (SMBBHs), formed in galaxy mergers, are the loudest sources of low-frequency GWs in the Universe (Centrella et al. 2010). Therefore, an intense electromagnetic search for wide and close systems in all stages of their evolution is currently ongoing (review by Komossa & Zensus 2016). While wide pairs can be identified by spatially resolved imaging spectroscopy, we rely on indirect methods of detecting the most compact, evolved systems. These are well beyond the 'final parsec' in their evolution (Begelman, Blandford & Rees 1980; Colpi 2014), in a regime where GW emission contributes to orbital shrinkage. Semiperiodicity in light curves has been a major tool for selecting small-separation SMBBH systems.

OJ 287 is a nearby, bright, and massive blazar at redshift $z = 0.306$ (Dickel et al. 1967), and among the best candidates to date for hosting a compact SMBBH (Sillanpaa et al. 1988; Valtonen et al. 2016). Its unique optical light curve spans more than a century, dating back to 1891. It shows pronounced optical double peaks every ∼12 yr, which have been interpreted as arising from the orbital motion of a pair of SMBHs, with an orbital period on that order (∼9 yr in the system's rest frame).

While different variants of binary scenarios have been discussed in the past (e.g. Lehto & Valtonen 1996; Katz 1997; Villata et al. 1998; Liu & Wu 2002; Britzen et al. 2018; Dey et al. 2019), the best explored model explains the double peaks as the times when the secondary SMBH impacts the disc around the primary twice during its 12.06 yr orbit ('impact flares' hereafter). The most recent orbital two-body modelling is based on 4.5-order post-Newtonian dynamics and successfully reproduces the overall long-term light curve of OJ 287 until 2019 (Valtonen et al. 2016; Dey et al. 2018; Laine et al. 2020 and references therein). It requires a compact binary with a semimajor axis of 9300 au, which is subject to GR precession of $\Phi = 38$ deg/orbit, on an eccentric orbit ($\epsilon = 0.7$), with a massive primary of 1.8×10^{10} $M_\odot$ and a secondary of 1.5×10^8 $M_\odot$. Independent evidence for a massive primary comes from the host galaxy of OJ 287 and other arguments (e.g. Wright et al. 1998; Kushwaha et al. 2018a; Nilsson et al. 2020). We are carrying out a multiyear, multifrequency monitoring programme of OJ 287, in order to search for epochs of outbursts and explore facets of the binary SMBH model (for first results, see Komossa et al. 2017; Komossa, Grupe & Gomez 2018; Myserlis et al. 2019; Komossa, Grupe & Gomez 2020a). Independent

★ E-mail: astrokomossa@gmx.de

Table 1. Summary of X-ray observations (see Section 2 for UVOT data).

Mission	Band (keV)	Date (t_{start})	MJD	Δt (ks)
Swift XRT	0.3–10	2015 November–2020 June	57354–59012	0.5–2
XMM–Newton	0.2–10	2020 April 24	58963	15
NuSTAR	3–79	2020 May 4	58973	29

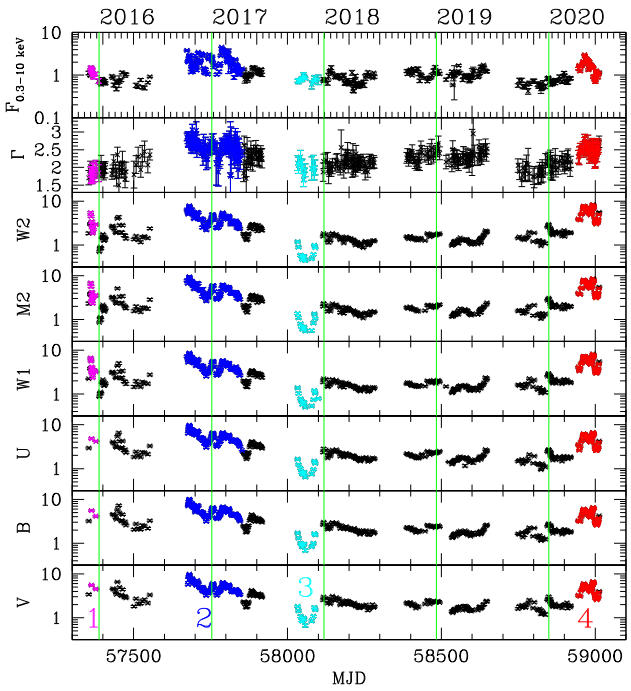

Figure 1. *Swift* X-ray to optical light curve of OJ 287 since the start of our monitoring, between 2015 December and 2020 June. The observed absorption-corrected X-ray flux (0.3–10 keV) and the extinction-corrected optical–UV fluxes are in units of 10^{-11} erg s^{-1} cm^{-2}. Γ_x is the X-ray power-law photon index. Four epochs of outbursts/low states are marked in colour: (1) a second peak of the 2015 centennial 'impact flare', (2) the 2016–2017 outburst, (3) a deep minimum state, and (4) the 2020 April–June outburst. The vertical green lines mark January 1 of each of the years between 2016 and 2020.

of the binary's presence, OJ 287 is a nearby bright blazar, and dense multifrequency monitoring and high-resolution X-ray spectroscopy are powerful diagnostics of jet and accretion physics in blazars.

Here, we present the detection of a bright outburst of OJ 287 in 2020 April–June with the Neil Gehrels *Swift* observatory (*Swift* hereafter; Gehrels et al. 2004), even brighter in UV–X-rays than the observed part of the 2015 'centennial' impact flare, and the second brightest in X-rays since the beginning of *Swift* observations of OJ 287 in 2005. *XMM–Newton* and *NuSTAR* X-ray spectroscopy was used in order to understand the nature of this outburst. (The long-term *Swift* light curve will be analysed further in upcoming work; paper II hereafter). We use a cosmology (Wright 2006) with $H_0 = 70$ km s^{-1} Mpc^{-1}, $\Omega_M = 0.3$, and $\Omega_\Lambda = 0.7$ throughout this paper.

2 DATA ANALYSIS AND SPECTRAL FITS

2.1 *Swift*

We have monitored OJ 287 since 2015 December (Table 1 and Fig. 1, which also includes some *Swift* data sets from other programmes and

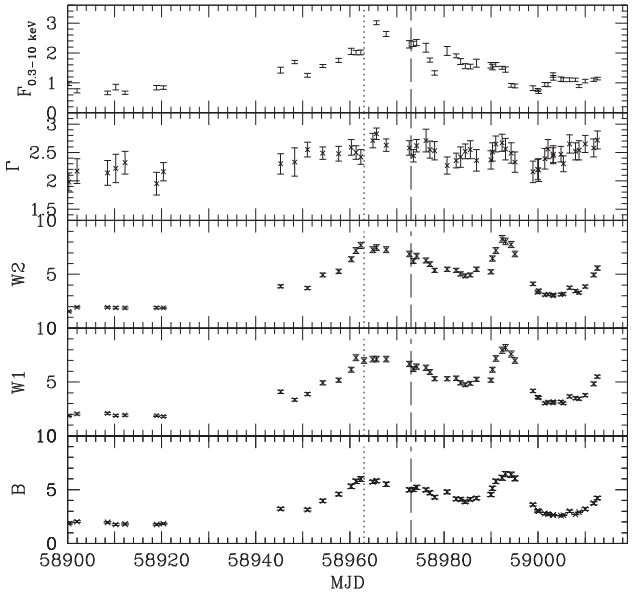

Figure 2. Zoom on the time interval around the 2020 outburst in selected bands (fluxes and units as in Fig. 1). The times of our *XMM–Newton* (dotted) and *NuSTAR* (dashed) observations are marked by vertical lines. The main outburst peaking in late April (MJD 58962), which is the focus of this letter, is followed by a shorter second flare that is seen in the optical–UV bands but is less pronounced in X-rays. The last data point is from 2020 June 12.

PIs). The 2020 April–May outburst was typically covered with a cadence of 1–3 d, while the cadence was ∼2–10 d at other epochs. Long gaps of several months occur each year when OJ 287 is in *Swift* Sun constraint.

Most of the time, the *Swift* X-ray Telescope (XRT; Burrows et al. 2005) was operating in photon counting mode with typical exposure times of 0.5–2 ks. For X-ray analysis, source photons were extracted within a circle of radius 47 arcsec (equivalent to 20 detector pixels). The background was determined in a nearby circular region of radius 236 arcsec. X-ray spectra in the band (0.3–10) keV were generated and then analysed with the software package XSPEC (version 12.10.1f; Arnaud 1996).

Spectra were fit with single power laws of photon index Γ_x adding Galactic absorption with a column density $N_{H,Gal} = 2.49 \times 10^{20}$ cm^{-2}. Photon indices range between $\Gamma_x = 1.6$ and 3.0 (Figs 1and 2), with a general trend of steepening as OJ 287 becomes X-ray brighter.

We also observed OJ 287 with the Ultraviolet/Optical Telescope (UVOT; Roming et al. 2005) and typically in all six filters [*V* (5468Å), *B* (4392Å), *U* (3465Å), *UVW1* (2600Å), *UVM2* (2246Å), and *UVW2* (1928Å), where values in parentheses are the filter central wavelengths] in order to obtain reliable spectral energy distribution information of this rapidly varying blazar. Observations in each filter were co-added using the task *uvotimsum*. Source counts in all six filters were then selected in a circle of radius 5 arcsec and the background was determined in a nearby region of radius 20 arcsec. The background-corrected counts were then converted into fluxes based on the latest calibration as described in Poole et al. (2008) and Breeveld et al. (2010). The UVOT data were corrected for Galactic reddening of $E_{(B-V)} = 0.0248$ (Schlegel, Finkbeiner & Davis 1998), with a correction factor in each filter according to equation (2) of Roming et al. (2009) and based on the reddening curves of Cardelli et al. (1989).

2.2 *XMM–Newton*

Our *XMM–Newton* (Jansen et al. 2001) observation of OJ 287 was carried out in small window mode for 15 ks from 2020 April 24 21:13:18 to 2020 April 25 01:23:18 UTC when OJ 287 was near the maximum of its outburst (observation id 0854591201). The effective exposure time was 9 ks, after removing an epoch of flaring particle background.

The *XMM–Newton* data were reduced using the Science Analysis Software (SAS) version 18.0.0. EPIC-pn and EPIC-MOS spectra were extracted in a circular region of 20 arcsec centred on the source position and background photons were collected in a nearby region of ∼50 arcsec for the pn and ∼100 arcsec for the MOS instruments. A light-curve analysis of the 2020 data did not reveal significant short-time variability beyond the 3σ level, and therefore the spectra were analysed as a whole without splitting into different flux states. Inspection of the RGS spectrum did not reveal significant narrow spectral features, and the data were not analysed further.

For further analysis, spectra were binned to a signal-to-noise ratio (SNR) of at least 6, and to oversample the instrumental resolution by a factor of 3, and fit with several emission models (Table 2) with absorption fixed to the Galactic value (modelled with TBnew; Wilms, Allen & McCray 2000) or left free (at $z = 0.306$). OJ 287 is a very bright X-ray source. Fitting is based on χ^2 statistics. Overall, the spectrum shows a very soft emission component, a harder component up to 10 keV, and possible spectral structure in the Fe line region (Figs 3 and 4). The latter is independently present in both the EPIC-pn and EPIC-MOS data. It is best fit by an absorption line of EW = 0.1 keV, at a rest-frame energy of 7.45 ± 0.05 keV. This would correspond to an outflow with a velocity of $0.067c$ assuming the line is produced by iron Fe XXVI or $0.1c$ if it is produced by Fe XXV. Adding a Gaussian absorption line to the best-fitting model improves the fit by $\Delta\chi^2 = 17$, for two degrees of freedom, which corresponds to a significance of $\sim 3.7\sigma$. However, after correcting for the number of trials, assuming 20 resolution elements between 7 and 10 keV for the EPIC cameras, the false alarm probability is raised to 4 per cent, so the line significance is $\sim 2\sigma$. Therefore, its presence has to be confirmed in deeper future observations. While single-component broad-band models are unsuccessful, the *XMM–Newton* spectrum is best fit by the curved log-parabola plus flat power-law model with cold absorption at the Galactic value (Table 2).

For comparison, previous observations of OJ 287 between 2005 and 2018 were extracted from the *XMM–Newton* archive [PIs: S. Ciprini (Ciprini et al. 2007), R. Edelson, S. Komossa/N. Schartel]. The EPIC-pn data were reduced similar to our 2020 observation and were fit with single or double power laws. During the 2020 observation, OJ 287 was in its highest state so far covered by *XMM–Newton* spectroscopy, and dominated by a strong soft emission component (Fig. 3).

2.3 *NuSTAR*

We observed OJ 287 with *NuSTAR* (Harrison et al. 2013). The observation (sequence-id 90601616002) was carried out on 2020 May 4 starting at 20:36:09 UTC with an effective exposure time of 29.5 ks for FPMA and 29.3 ks for FPMB. The data were reduced using the latest *NuSTAR* data analysis software (NUSTARDAS) version 1.9.2. Source photons were extracted in a circular region of 30 arcsec centred on the source position. Background photons were collected in a nearby region of radius ∼100 arcsec on the same chip. Spectra were binned to an SNR of at least 6, and to oversample the instrumental resolution by a factor of 3. We fit the spectra separately and we allow for a difference in normalization and index between the two detectors. As this difference is small (< 1 per cent), we report only the FPMA values. Source emission is detected out to ∼70 keV, with a 2σ detection above 40 keV. The *NuSTAR* spectrum is well fitted with a single power-law model (Table 2), without any significant residuals. No strong Fe absorption line is detected. Its presence in both *XMM* spectra, or its faintness in the later *NuSTAR* spectrum, therefore is either a statistical fluctuation, or else the feature is short lived, or Fe becomes completely ionized as the flare continues and thus escapes detection with *NuSTAR*. There is a hint that the *NuSTAR* spectrum flattens at high energies, but adding a second power law does not improve the fit and the parameters cannot be constrained.

3 RESULTS AND DISCUSSION

3.1 Timing and spectroscopy

Four epochs stand out in our *Swift* light curve of OJ 287 (Fig. 1): (1) The (late phase of) the December 2015 'centennial flare', interpreted as the disc crossing of the secondary SMBH based on higher cadence optical data (Valtonen et al. 2016, 2019). (2) The long-lasting 2016–2017 flare that was the brightest in X-rays with *Swift* and with a soft spectrum (Verrecchia et al. 2016; Grupe, Komossa & Falcone 2017; Komossa et al. 2017; Kapanadze et al. 2018; Kushwaha et al. 2018b). The event was accompanied by a very high energy detection (VERITAS Collaboration 2017). (3) A sharp and symmetric deep low state in late 2017 in all optical (Valtonen et al. 2020) and UV bands, which is absent in X-rays (to be discussed further in paper II). (4) The 2020 April outburst, where OJ 287 reached the second-brightest X-ray state during the *Swift* monitoring. Here, our focus is the 2020 outburst, and X-ray analysis has been done with the following key questions in mind:

What does the variability imply about the emission site? At a mass of 1.8×10^{10} $M_\odot$, an innermost stable circular orbit of $R_{\rm ISCO} \sim 3R_{\rm S}$ corresponds to a minimum *rest-frame* light crossing time-scale of 6.3 d, which is larger than observed. Daily changes including a factor of 1.7 drop in flux within 2 d during the 2020 outburst (Fig. 2) therefore imply an emission site smaller than the last stable orbit of the primary SMBH of OJ 287, then indicating jet activity.

Is there any wavelength-dependent delay in the peak time of the flare? The UV–optical light curves follow each other closely and reach their peak quasi-simultaneously (see paper II for details), implying co-spatial emission and small opacities. X-rays follow substructure in the April flare closely, but the 2-week flat plateau does not allow to locate the peak precisely.

Which mechanism drives the softness of the X-ray spectrum: accretion or jet (synchrotron) activity? The very soft X-ray emission component could potentially represent emission associated with the inner accretion disc: either a high-energy tail of the big blue bump or reprocessing/reflection of coronal photons off the inner disc. Near the peak of the 2020 flare, the observed power-law flux corresponds to an *isotropic* X-ray luminosity of 10^{45} erg s^{-1}, which would imply an X-ray Eddington ratio of $L/L_{\rm Edd} = 4 \times 10^{-4}$ (8×10^{-2}) for a BH of mass 1.8×10^{10} $M_\odot$ (10^8 $M_\odot$) if it was accretion driven. Given the rapid variability, it then has to be the disc of the secondary BH. However, there is no other evidence so far for a long-lasting disc around the secondary, and the quasi-simultaneous variability in all bands from the optical to X-rays strongly argues for a synchrotron origin of the emission.

Even though blazars often show a synchrotron component in the X-ray band (Urry et al. 1996; Donato, Sambruna & Gliozzi 2005), it is interesting to note that their synchrotron component is rarely as

Table 2. Results from *XMM–Newton* and *NuSTAR* spectral fits. Absorption was fixed at the Galactic value $N_{\rm H,Gal}$, except when noted otherwise. Parameters and abbreviations are as follows: (1) models: pl = power law, bbdy = blackbody, logpar = logarithmic parabola model; (2) absorption in units of 10^{20} cm^{-2}; (3) power-law photon index; (4) unabsorbed power law or log-parabola flux from 0.5 to 10 keV in units of 10^{-12} erg s^{-1} cm^{-2}; (5) $kT_{\rm BB}$ in units of keV; (6) bbdy emission in units of $10^{-5} \times (L/10^{39}$ erg s$^{-1})/[(D/10$ kpc$)(1+z)]^2$, where L and D are the source luminosity and distance; (7) curvature parameter β and (8) spectral index α of the log-parabola model; (9) goodness of fit χ^2 and number of degrees of freedom. For *NuSTAR* data, the pl flux is given from 3 to 50 keV. When no errors are reported, the quantity was fixed.

Model (1)	$N_{\rm H}$ (2)	Γ_1 (3)	f_1 (4)	Γ_2 (3)	f_2 (4)	kT (5)	$f_{\rm BB}$ (6)	β (7)	α (8)	$f_{\rm lp}$ (4)	$\chi^2/n_{\rm dof}$ (9)
XMM											
pl	2.49	2.82 ± 0.01	38.5 ± 0.1	–	–	–	–	–	–	–	476/284
pl + pl	2.49	2.84 ± 0.01	38.1 ± 0.2	0.0 ± 0.4	$0.9^{+0.2}_{-0.1}$	–	–	–	–	–	380/282
pl + pl, $N_{\rm H}$ free	$3.4^{+0.9}_{-0.8} + 2.49$	3.1 ± 0.1	38.0 ± 1.0	$1.7^{+0.2}_{-0.3}$	5^{+3}_{-2}	–	–	–	–	–	343/281
pl + bbdy	2.49	2.70 ± 0.01	35.2 ± 0.3	–	–	0.152 ± 0.003	8.0 ± 0.7	–	–	–	343/282
pl + pl + bbdy	2.49	2.76 ± 0.03	35.6 ± 0.3	0 ± 1	$0.6^{+0.4}_{-0.2}$	0.16 ± 0.01	6.0 ± 1.0	–	–	–	311/280
logpar + pl	2.49	2.2	17.3 ± 0.6	–	–	–	–	0.8 ± 0.1	3.22 ± 0.03	9.1 ± 0.3	286/282
NuSTAR											
pl	2.49	2.36 ± 0.06	6.1 ± 0.2	–	–	–	–	–	–	–	74/74
pl (> 10 keV)	2.49	2.2 ± 0.2	–	–	–	–	–	–	–	–	–

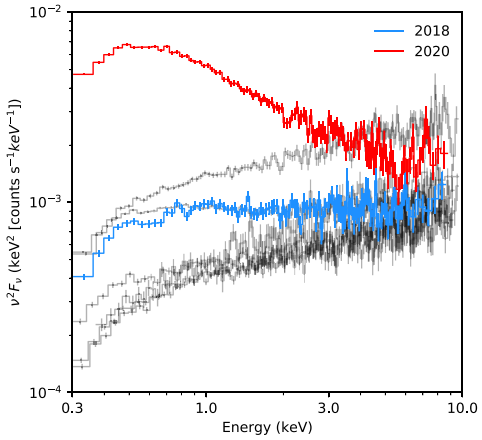

Figure 3. Comparison of all *XMM–Newton* (EPIC-pn) spectra of OJ 287 between 2005 and 2020 (corrected for effective area of the detector, and without applying any model fits). Our 2020 and 2018 data are highlighted in red and blue, respectively. A strong soft emission component dominates the 2020 spectrum.

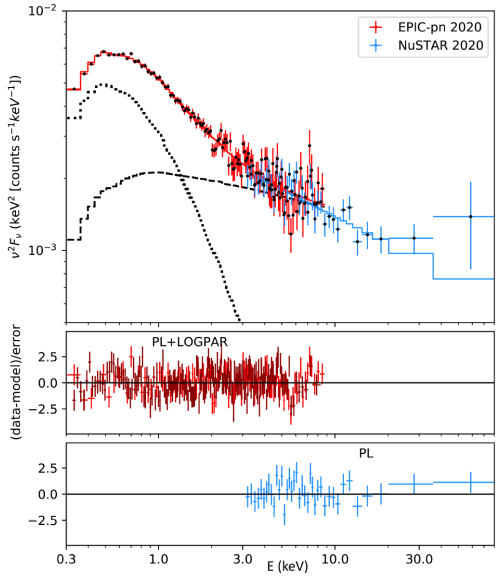

Figure 4. Best-fitting log-parabola plus power-law model of OJ 287 observed with *XMM–Newton*, folded with the instrumental response and uncorrected for Galactic absorption. The dotted and dashed lines represent the log-parabola and power-law contributions, respectively. The *NuSTAR* data and fit are added to the plot. The second panel displays the residuals for the best-fitting log-parabola model (pn and MOS data), while the third panel displays the residuals of the *NuSTAR* fit.

soft as in OJ 287 (see paper II for further discussion). We find that OJ 287 generally exhibits a 'softer-when-brighter' variability pattern in our multiyear *Swift* light curve[1] – with the exception of the epoch around the 2015 impact flare when the X-ray spectrum was rather hard.

In summary, the various observations imply that the 2020 April outburst is not dominated by accretion disc emission but rather by non-thermal emission from the jet, further corroborated by the Effelsberg detection of a (delayed) radio flare (Komossa et al. 2020b), and by the detection of high polarization of the optical flare of OJ 287 first reported by Zola et al. (2020).

3.2 Binary BH model

In the context of the binary SMBH model for OJ 287 as reviewed by Dey et al. (2019), there are several potential sites of UV–X-ray emission, which may become bright at different epochs: First, the impact flare (bremsstrahlung) from the secondary, as it impacts the accretion disc around the primary, causing a two-sided expanding bubble (Ivanov, Igumenshchev & Novikov 1998). It was last observed in 2019 July (Laine et al. 2020) and none is predicted for 2020. Secondly, temporary accretion and perhaps jet emission of the secondary SMBH while and/or after passing the primary's disc (Pihajoki et al. 2013). However, it is unlikely that any secondary SMBH of much lower mass and different spin, and with a temporary disc without large-scale magnetic field, will trigger *synchrotron flares* of very similar brightness and spectrum as the primary (see the long-term light curve in Fig. 1). Thirdly, 'after-flares' in form of changes in the accretion rate of the primary, after the impact disturbance has travelled to the inner edge of the accretion disc, then later followed by changes in jet activity in response.

[1]Also seen on long time-scales when combining a few *Einstein*, *EXOSAT*, *ROSAT*, and *ASCA* data (Isobe et al. 2001; but see Seta et al. 2009).

Sundelius et al. (1997) (see also Valtonen et al. 2009) predicted the expected after-flares of OJ 287 tidally induced by the secondary. Based on their model, we expect major *accretion* after-flare activity in early 2020 January. Relating their predicted (accretion) peak in 2020 January with the (jet) outburst reported here in April requires a time delay of ∼4 months between *accretion disc* and *jet* activity, and implies rapid communication between disc and jet. Factors that determine the actual delay between accretion and jet changes include the disc/corona properties and geometry, the magnetic field geometry, and shock formation in the jet (e.g. Tchekhovskoy et al. 2014; Marscher et al. 2018; Valtonen et al. 2019), which are not yet well understood, and we therefore cannot predict delays from first principles, but can compare with other extragalactic systems where delays were observed. Overall, the time-scale observed in OJ 287 is consistent with the one seen in stellar tidal disruption events (Komossa & Zensus 2016) where accretion flares are typically followed by detectable radio-jet activity within days (e.g. Zauderer et al. 2011), and with the blazar 3C 120 for which Marscher et al. (2002) reported a delay of 0.1 yr between accretion and radio-jet activity.

4 SUMMARY AND CONCLUSIONS

We have monitored OJ 287 with *Swift* since 2015 December, revealing multiple epochs of high-amplitude optical–X-ray variability. The bright 2020 April–June super-outburst of OJ 287 has one of the densest quasi-simultaneous optical–UV–X-ray coverages obtained so far for this blazar. We also presented the first *XMM–Newton* and *NuSTAR* broad-band X-ray spectroscopy of OJ 287 in outburst.

Several X-ray spectral features stand out: First, a steep low-energy component ($\Gamma_x = 2.8$) at peak, rarely that soft in blazars but consistent with a synchrotron origin. Across the flare, OJ 287 is softer when brighter, a pattern also seen in our long-term *Swift* light curve. Secondly, a power-law component detected up to ∼70 keV ($\Gamma_x \sim 2.4$). Thirdly, signs of reprocessing in the Fe line region, which may represent a relativistic outflow if confirmed.

We find that the outburst is jet-driven and consistent with a binary SMBH model, where the disc impact of the secondary BH triggers an after-flare in form of time-delayed accretion activity on the primary, which is then followed by an increase in jet emission of the primary ∼4 months later.

ACKNOWLEDGEMENTS

We would like to thank the *Swift*, *XMM–Newton* and *NuSTAR* teams for carrying out our observations, and our anonymous referee for very useful comments.

DATA AVAILABILITY STATEMENT

Data are available on request.

REFERENCES

Abbott B. P. et al., 2016, Phys. Rev. Lett., 116, 061102
Abbott B. P. et al., 2019, ApJ, 882, L24
Arnaud K. A., 1996, in Jacoby G. H., Barnes J.eds, ASP Conf. Ser. Vol. 101, Astronomical Data Analysis Software and Systems V. Astron. Soc. Pac., San Francisco, p. 17
Begelman M. C., Blandford R. D., Rees M. J., 1980, Nature, 287, 307
Breeveld A. A. et al., 2010, MNRAS, 406, 1687
Britzen S. et al., 2018, MNRAS, 478, 3199
Burrows D. N. et al., 2005, Space Sci. Rev., 120, 165
Cardelli J. A., Clayton G. C., Mathis J. S., 1989, ApJ, 345, 245
Centrella J., Baker J. G., Kelly B. J., van Meter J. R., 2010, Rev. Mod. Phys., 82, 3069
Ciprini S. et al., 2007, Mem. Soc. Astron. Ital., 78, 741
Colpi M., 2014, Space Sci. Rev., 183, 189
Dey L. et al., 2018, ApJ, 866, 11
Dey L. et al., 2019, Universe, 5, 108
Dickel J. R. et al., 1967, AJ, 72, 757
Donato D., Sambruna R. M., Gliozzi M., 2005, A&A, 433, 1163
Gehrels N. et al., 2004, ApJ, 611, 1005
Grupe D., Komossa S., Falcone A., 2017, Astron. Telegram, 10043, 1
Harrison F. A. et al., 2013, ApJ, 770, 103
Isobe N., Tashiro M., Sugiho M., Makishima K., 2001, PASJ, 53, 79
Ivanov P. B., Igumenshchev I. V., Novikov I. D., 1998, ApJ, 507, 131
Jansen F. et al., 2001, A&A, 365, L1
Kapanadze B., Vercellone S., Romano P., Hughes P., Aller M., Aller H., Kapanadze S., Tabagari L., 2018, MNRAS, 480, 407
Katz J. I., 1997, ApJ, 478, 527
Komossa S., Zensus J. A., 2016, Proc. IAU Symp. 312, Star Clusters and Black Holes in Galaxies Across Cosmic Time. Kluwer, Dordrecht, p. 13
Komossa S. et al., 2017, Proc. IAU Symp. 324, New Frontiers in Black Hole Astrophysics. Kluwer, Dordrecht, p. 168
Komossa S., Grupe D., Gomez J. L., 2018, Astron. Telegram, 12086, 1
Komossa S., Grupe D., Gomez J. L., 2020a, Astron. Telegram, 13658, 1
Komossa S., Kraus A., Grupe D., Dey L., Gomez J. L., Gopakumar A., Parker M., Valtonen M., 2020b, Astron. Telegram, 13702, 1
Kushwaha P. et al., 2018a, MNRAS, 473, 1145
Kushwaha P. et al., 2018b, MNRAS, 479, 1672
Laine S. et al., 2020, ApJ, 894, L1
Lehto H. J., Valtonen M. J., 1996, ApJ, 460, 207
Liu F. K., Wu X. B., 2002, A&A, 388, L48
Marscher A. P., Jorstad S. G., Gómez J. L., Aller M. F., Teräsranta H., Lister M. L., Stirling A. M., 2002, Nature, 417, 625
Marscher A. P. et al., 2018, ApJ, 867, 128
Myserlis I. et al., 2019, A&A, 619, 88
Nilsson K. et al., 2020, A&A , submitted
Pihajoki P. et al., 2013, ApJ, 764, 5
Poole G. B., Babul A., McCarthy I. G., Sanderson A. J. R., Fardal M. A., 2008, MNRAS, 391, 1163
Roming P. W. A. et al., 2005, Space Sci. Rev., 120, 95
Roming P. W. A. et al., 2009, ApJ, 690, 163
Schlegel D. J., Finkbeiner D. P., Davis M., 1998, ApJ, 500, 525
Seta H. et al., 2009, PASJ, 61, 1011
Sillanpaa A., Haarala S., Valtonen M. J., Sundelius B., Byrd G. G., 1988, ApJ, 325, 628
Sundelius B., Wahde M., Lehto H. J., Valtonen M. J., 1997, ApJ, 484, 180
Tchekhovskoy A., Metzger B. D., Giannios D., Kelley L. Z., 2014, MNRAS, 437, 2744
Urry C. M., Sambruna R. M., Worrall D. M., Kollgaard R. I., Feigelson E. D., Perlman E. S., Stocke J. T., 1996, ApJ, 463, 424
Valtonen M. J. et al., 2009, ApJ, 698, 781
Valtonen M. J. et al., 2016, ApJ, 819, L37
Valtonen M. J. et al., 2019, ApJ, 882, 88
Valtonen M. J. et al., 2020, submitted
Verrecchia F., Ciprini S., Valtonen M., Zola S., 2016, Astron. Telegram, 9709, 1
VERITAS Collaboration, 2017, Astron. Telegram, 10051, 1
Villata M., Raiteri C. M., Sillanpaa A., Takalo L. O., 1998, MNRAS, 293, L13
Wilms J., Allen A., McCray R., 2000, ApJ, 542, 914
Wright E. L., 2006, PASP, 118, 1711
Wright S. C., McHardy I. M., Abraham R. G., Crawford C. S., 1998, MNRAS, 296, 961
Zauderer B. A. et al., 2011, Nature, 476, 425
Zola S. et al., 2020, Astron. Telegram, 13637, 1

This paper has been typeset from a TEX/LATEX file prepared by the author.